ACS APPLIED MATERIALS & INTERFACES

Research Article

www.acsami.org

Construction of Heterostructured g-C_3N_4/Ag/TiO_2 Microspheres with Enhanced Photocatalysis Performance under Visible-Light Irradiation

Yanfeng Chen, Weixin Huang, Donglin He, Yue Situ,* and Hong Huang*

School of Chemistry and Chemical Engineering, South China University of Technology, Guangzhou 510640, People's Republic of China

Supporting Information

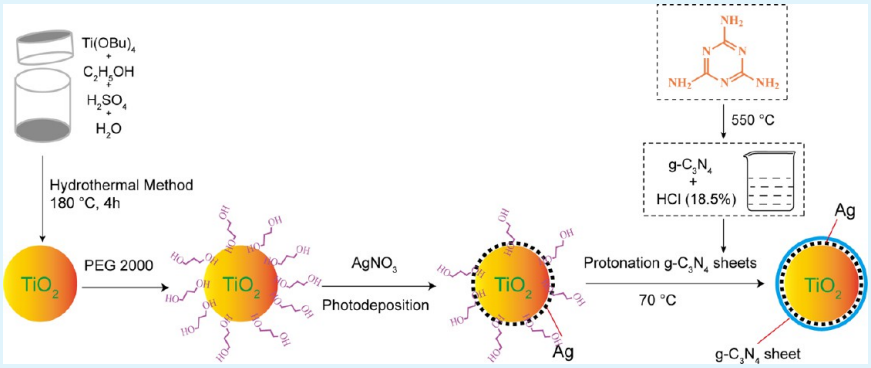

ABSTRACT: The visible-light photocatalytic performance of the heterostructured g-C_3N_4/Ag/TiO_2 microspheres was investigated. As an electron-conduction bridge, Ag nanoparticles were photodeposited as the interlayer between g-C_3N_4 and the surface of TiO_2 microspheres to increase visible-light absorption via the surface plasmon resonance. The interface between Ag/TiO_2 and g-C_3N_4 facilitates the direct migration of photoinduced electrons from g-C_3N_4 to Ag/TiO_2, which is conductive to retarding the recombination of electron−holes. The g-C_3N_4 (4%)/Ag/TiO_2 microsphere sample shows significant photocatalytic activity, higher than the sum of g-C_3N_4 (1.2 mg) and Ag/TiO_2 samples, or the sum of TiO_2 and Ag/g-C_3N_4 (1.8 mg) samples. It indicates that the heterostructured combination of g-C_3N_4, Ag and TiO_2 microspheres provides synergistic photocatalytic activity through an efficient electron transfer process.

KEYWORDS: *heterostructured, g-C_3N_4, Ag, TiO_2 microspheres, photocatalysis, visible-light*

1. INTRODUCTION

With increasing environmental problems and the energy crisis, photocatalytic degradation of organic pollutants or hydrogen production from water splitting over a semiconductor is one of the most important technologies for further maximizing the efficiency of solar energy.[1−3] Titanium dioxide (TiO_2) has been considered as one of the most promising semiconductor materials due to its unique characteristics like high photocatalytic activity, low cost, stability and nontoxicity. Nevertheless, its inherent drawbacks in photocatalysis are the low solar energy utilization efficiency because of its wide band gap (3.20 eV) and rapid recombination of photoinduced electron−holes, which largely limit its applications.[4] Therefore, it is of great significance to develop new TiO_2 photocatalysts with visible-light response by enhancing light harvesting, efficient photoexcited charge separation and reducing the recombination of the photoinduced electron−holes.

Numerous attempts have been dedicated to increasing the photocatalytic efficiency of TiO_2 including chemical modification, surface sensitization and coupling with other semiconductor materials.[5−8] Recently, much interest has been focused on doping TiO_2 with g-C_3N_4, which extends its absorption to the visible-light region, owing to the special electronic band structure.[9−12] In the photocatalyst system of g-C_3N_4/TiO_2 composites, the photoinduced holes tend to pass from the valence band (VB) of TiO_2 to the VB of g-C_3N_4 under UV irradiation, while the electrons pass from the conduction band (CB) of g-C_3N_4 to the CB of TiO_2.[13] However, in the case of visible-light irradiation, TiO_2 can only generate electrons, which results in a slow electron transfer from g-C_3N_4 to TiO_2 and a high recombination of hole−electrons. To overcome the fast recombination process, considerable research has been carried out using a noble metallic combination of semiconductors.[14,15] In the case of a Ag/TiO_2 composite, the main role of metallic Ag was taken as follows: (i) Ag serves as electron sinks, to facilitate the transfer of interfacial electron in the composite; (ii) the composite strongly absorbs visible light because of the surface plasmon resonance of Ag.[16,17]

Herein, a novel ternary composite of heterostructured g-C_3N_4/Ag/TiO_2 microspheres was prepared, and the metallic

Received: June 11, 2014
Accepted: August 4, 2014
Published: August 4, 2014

Ag was photodeposited as the interlayer between g-C_3N_4 and TiO_2. The structure of the as-prepared TiO_2 microspheres, Ag/TiO_2 microspheres, g-C_3N_4/TiO_2 microspheres and g-C_3N_4/Ag/TiO_2 microspheres were investigated by scanning electron microscopy (SEM). The heterostructure of g-C_3N_4/Ag/TiO_2 microspheres was further investigated by transmission electron microscopy (TEM). The surface composition and chemical status of elements in the as-prepared g-C_3N_4/Ag/TiO_2 microspheres were characterized by X-ray photoelectron spectroscopy (XPS). The composites exhibited much higher photocatalytic activity for degrading methyl orange or phenol than the bare TiO_2 or g-C_3N_4 under visible-light irradiation (>420 nm), distinctly demonstrating that the existence of a synergistic effect between Ag/g-C_3N_4 and TiO_2 as well as Ag/TiO_2 and g-C_3N_4. The low recombination of the prepared g-C_3N_4/Ag/TiO_2 microspheres was determined based on a photoluminescence (PL) technique. In addition, the possible photocatalysis mechanism of g-C_3N_4/Ag/TiO_2 microspheres under visible light was also discussed.

2. EXPERIMENTAL SECTION

Materials. Melamine ($C_3H_6N_6$, 99.0%) was purchased from Chengdou Kelong Chemical Reagent Co., China. Tetrabutyl titanate (Ti $(OC_4H_9)_4$, 98.5%) was obtained from Jiangsu Yonghua Fine Chemicals Co., China. Concentrated hydrochloric acid (HCl, 36.0−38.0%) and concentrated sulfuric acid (H_2SO_4, 98.0%) were obtained from Guangzhou Chemical Reagent Co., China. Polyethylene glycol (PEG, M = 2000) was purchased from Guangdong Guanghua Chemical Reagent Co., China. Silver nitrate ($AgNO_3$, ≥99.0%) was obtained from Shanghai Fine Chemical Materials Research Institution. All chemical reagents were used without further purification.

Preparation of Protonation g-C_3N_4 Sheets. Graphite-like C_3N_4 sheets were synthesized on the basis of a procedure reported previously.[18] Specifically, 5.0 g of melamine was calcined at 550 °C for 4 h with a heating rate of 2 °C/min in a muffle furnace. The obtained yellow agglomerate was ground into powder. 1.0 g of the g-C_3N_4 sheets were treated by a postprocessing with HCl (18.5 wt %, 50 mL) for 4 h of protonation at room temperature.[19] Before being filtered, the g-C_3N_4/HCl/H_2O suspension was diluted with 500 mL of deionized water. Then the protonated g-C_3N_4 was washed with deionized water until neutral conditions and dried at 105 °C in air for 4 h. 100 mg of the as-prepared protonated g-C_3N_4 sheets was ultrasonically dispersed in deionized water for 6 h to get well-dispersed aqueous solution of 1 mg mL^{-1}.

Preparation of TiO_2 Microspheres. In a typical hydrothermal method,[20] 0.26 mL of concentrated sulfuric acid (98.0%) and 0.24 mL of deionized water were added, in order, to a homogeneous yellow solution, which was obtained by mixing 4.0 g of Ti $(OC_4H_9)_4$ with 60 mL of anhydrous ethanol. Subsequently, the obtained solution was moved to a 100 mL Teflon lined stainless steel autoclave and kept at 180 °C for 4 h. The as-synthesized product was isolated by centrifugation, washed with anhydrous ethanol three times and dried at 60 °C for 24 h in a vacuum oven.

Preparation of g-C_3N_4/Ag/TiO_2 Microspheres. The as-prepared TiO_2 microspheres (300 mg) were mixed with 200 mL of deionized water by ultrasonication for 30 min. Then, 1.0 mL of 5% polyethylene glycol (PEG) 2000 solution was added and the dispersion was stirred for another 10 min.[21,22] For deposition of silver on the surface of TiO_2 microspheres, a photodeposition method was applied as follows: 3.5 mL of $AgNO_3$ solution (2.754 mg mL^{-1}) was added to the dispersion. Then the suspension was transferred to a water-cooled reactor (250 mL) and irradiated under a PLS-SXE300 Xe lamp with 100 mW cm^{-2} illumination intensity for 60 min. The theoretical value of Ag loading amount was 2 wt %.[20,23,24] For further wrapping g-C_3N_4 on Ag/TiO_2 microspheres, a certain amount (6, 12 and 18 mL) of the protonated g-C_3N_4 sheets solution (1 mg mL^{-1}) was added and the reaction temperature was kept at 70 °C for 60 min. The resulting suspension was filtered, washed with deionized water three times and dried at 60 °C for 24 h in a vacuum oven. The theoretical wrapping amount of g-C_3N_4 was 2, 4 and 6 wt %. For comparison, Ag (2 wt %)/TiO_2 microspheres were prepared without the wrapping process of g-C_3N_4, g-C_3N_4 (4 wt %)/TiO_2 microspheres were prepared without the depositing process of silver and Ag/g-C_3N_4 (1:2) sample was prepared without adding TiO_2 microspheres.

Characterization. The crystal forms of these materials were tested by X-ray diffracttion (XRD, Bruker D8 ADVANCE) with Cu Kα radiation (1.541 78 Å). The morphologies of the pure TiO_2 microspheres, Ag/TiO_2 microspheres, g-C_3N_4/TiO_2 microspheres and g-C_3N_4 (2, 4 and 6%)/Ag/TiO_2 microspheres were examined by scanning electron microscopy (SEM, LEO 1530 VP). The interlayer structure of g-C_3N_4 (4%)/Ag/TiO_2 microspheres was conducted with transmission electron microscopy (TEM, JEOL, JEM-2100F, 200 kV, Japan). The g-C_3N_4 (4%)/Ag/TiO_2 microspheres were embedded in EPON RESIN 812 (Fenwal Inc., Lake Zurich, IL, USA). Ultrathin sections (90−150 nm) were cut on an ultramicrotome (Leica UC6+FC6, Wetzlar, Austria) with diamond knives. The ultrathin sections were placed on a lacey carbon film 200 mesh copper TEM grid. Fourier transform-infrared (FT-IR) spectra of the samples were recorded on a Bruker Vector 33 spectrometer. Surface chemical compositions and chemical status in the as-prepared materials were analyzed by X-ray photoelectron spectroscopy (XPS, VG Scientific ESCA LAB MK II or a Thermo ESCALAB 250Xi). UV−vis diffuse reflectance spectra were recorded in a Hitachi Corporation UV-3010 spectrophotometer ($BaSO_4$ as a reflectance standard). Photoluminescence (PL) spectra were measured at room temperature on an F-5400 fluorescence spectrophotometer (Hitachi, Japan) with an excitation wavelength of 325 nm. The scanning speed was 1200 nm min^{-1}, and the photomultiplier voltage was 700 V. The widths of the excitation and emission slits were 2.5 and 5.0 nm. Nitrogen adsorption−desorption isotherms were obtained from a TriStar 3010 isothermal nitrogen sorption analyzer (Micromeritics, USA). The concentration of total organic carbon (TOC) was analyzed by a TOC-V_{CPN} Analyzer (TOC-V_{CPN}, Shimadzu Corporation, Japan).

Assessment of Photocatalytic Activities and Detection of Hydroxyl Radicals. The photocatalytic activities of the materials were evaluated by degrading methyl orange (13.5 mg L^{-1}) or phenol (16.6 mg L^{-1}) in H_2O. Thirty milligrams of the as-prepared powder was combined with 30 mL of the organic substance solution in a 50 mL triangular flask and was stirred for 30 min to reach the desorption−absorption equilibrium in a dark box. The suspension was transferred to a water-cooled reactor and irradiated under visible light by using a PLS-SXE300 Xe lamp (Beijing Perfectlight Technology Co., Ltd.) with a 420 nm cutoff filter. Three milliliter aliquots were collected at certain time intervals and then filtered with a microspore filter (0.22 μm) to remove the as-prepared photocatalysts. The filtrate was measured by a Shimadzu UV-2050 spectrophotometer to record the maximum absorbance (462 nm for methyl orange and 270 nm for phenol).

The formation of hydroxyl radicals (·OH) of the as-prepared samples was detected by a photoluminescence (PL) method using terephthalic acid (TA) as a probe molecule.[25] Thirty milligrams of the as-prepared sample was dispersed in the aqueous solution (30 mL) containing 5×10^{-4} mol L^{-1} TA and 2×10^{-3} mol L^{-1} NaOH. The Xe lamp irradiation with different light filters (full spectrum or visible-light) was continuous. Sampling was conducted every 1 h for analysis. The solution was measured after filtration on an F-5400 fluorescence spectrophotometer. TA hydroxylation gave a PL peak at 435 at 315 nm light excitation.

3. RESULTS AND DISSCUSSION

Crystal Structures. The XRD patterns of the prepared samples are shown in Figure 1. It is obvious that the pure TiO_2 and TiO_2 composite microspheres with different components exhibit similar diffraction patterns. The peaks at around 2θ = 25.3°, 37.8°, 47.9°, 53.8°, 55.1°, 62.7°, 68.7°, 70.3° and 75.0° are attributed to the (101), (004), (200), (105), (211), (204),

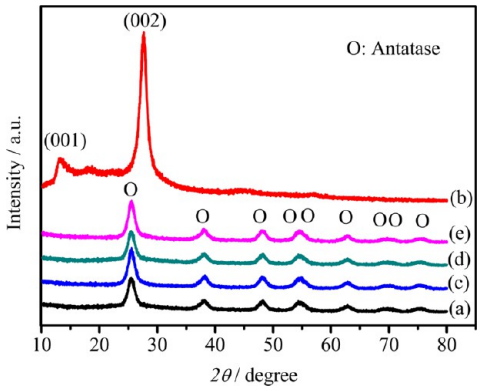

Figure 1. XRD patterns of TiO_2 microspheres (a), protonated g-C_3N_4 (b), g-C_3N_4/TiO_2 microspheres (c), Ag/TiO_2 microspheres (d) and g-C_3N_4 (4%)/Ag/TiO_2 microspheres (e).

(116), (220) and (215) crystal planes of anatase TiO_2 in pure TiO_2 microspheres, respectively.[26] As shown in Figure 1b, the peak at 2θ value of 13.1° corresponds to (100) crystal plane of tri-s-triazine units, whereas the peak at 27.4°, indexed as (002) crystal plane, is attributed to interlayer stacking of aromatic segments.[27] It should be noted that no typical diffraction peaks of g-C_3N_4 or Ag appear in the g-C_3N_4/TiO_2 composite microspheres, Ag/TiO_2 composite microspheres and g-C_3N_4 (4%)/Ag/TiO_2 composite microspheres. The reason can be ascribed to low weight loading of g-C_3N_4 or Ag on the surface of the TiO_2 composite microspheres.[28]

Morphology Characterizations. The g-C_3N_4/Ag/TiO_2 microspheres were prepared by two main processes, as illustrated in Figure 2. The first step was taken to prepare Ag (2 wt %)/TiO_2 microspheres. On this basis, the second step was taken to wrap g-C_3N_4 on the surface of Ag/TiO_2 microspheres. As shown in Figures 3a and S1 (a) (Supporting Information), the SEM images of pure TiO_2 microspheres shows a smooth surface, whereas a loose structure formed by TiO_2 nanoparticles with diameters of about 10 nm can be observed in its enlarged view. To get a well-dispersed g-C_3N_4 aqueous solution, g-C_3N_4 was protonated with concentrated HCl solution.[19] It is clearly shown in Figure 3b that the protonated g-C_3N_4 with a breaking up of stacks and the small g-C_3N_4 particles would be in favor of g-C_3N_4 wrapping on the surface of TiO_2 microspheres. The purpose of the addition of PEG 2000 aqueous solution is to introduce the hydroxyl groups to the surface of TiO_2 microspheres.[21,22] As shown in Figure 3c, g-C_3N_4 was coated on TiO_2 microspheres with a wrapping amount of 4 wt %. The diameters of the g-C_3N_4/TiO_2 microspheres show no obvious change, which indicates that the size controlling effect exists in the encapsulating process of g-C_3N_4. This was because of PEG 2000 as a stabilizing surfactant and protonated g-C_3N_4 with the small breaking up of stacks, which were effective to confine the particle shape. In the process of photodeposition, a large amount of nano-Ag particles were formed on the surface of TiO_2 microspheres after UV irradiation in the presence of $AgNO_3$. With a Ag-loading amount of 2 wt %, the surface of the TiO_2 microspheres becomes rough and dark, compared to that of the pure TiO_2 microspheres (Figure 3d). Figure S1 (d) (Supporting Information) demonstrates that stacked nanoparticles are present on Ag/TiO_2 microsphere surfaces and are denser than those in Figure S1 (a) (Supporting Information), suggesting the homogeneous distribution of nano-Ag particles on the TiO_2 surface. Survey SEM image of g-C_3N_4 (4%)/Ag/TiO_2 microspheres is shown in Figure S2 (Supporting Information). The diameters of the as-prepared g-C_3N_4 (4%)/Ag/TiO_2 microspheres are in the range of 2−5 μm. The micromorphology of g-C_3N_4/Ag/TiO_2 microspheres with different wrapping amounts of g-C_3N_4 (2, 4 and 6%) are exhibited in Figure 3e1−e3. The low percentage (2%) of g-C_3N_4 in the Ag/TiO_2 microspheres did not lead to the complete encapsulation on the surface of Ag/TiO_2 microspheres (Figure 3e1). In contrast, in Figure 3e2,e3, the surface of Ag/TiO_2 microspheres was completely encapsulated by g-C_3N_4. These features suggest that the as-prepared g-C_3N_4/Ag/TiO_2 microspheres have a promising structure of g-C_3N_4−Ag−TiO_2 for visible light photocatalysis, because the interlayer Ag nanoparticles act as a bridge to facilitate the efficient electron transportation and compress the electron−holes recombination.

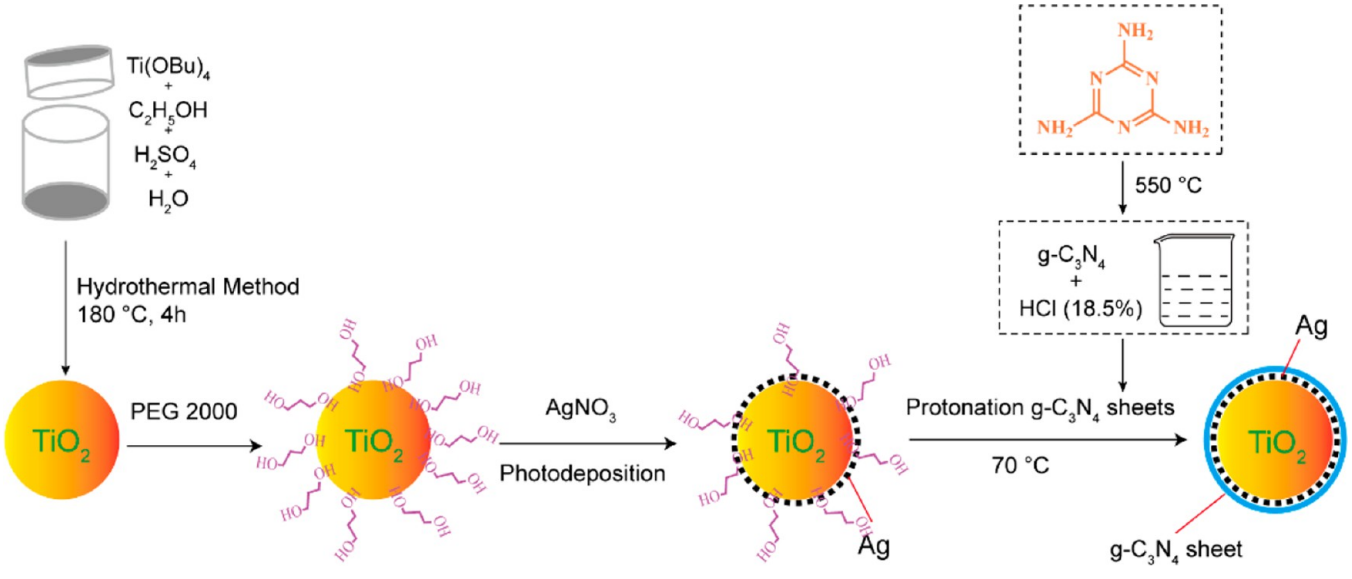

Figure 2. Schematic illustration for the preparation of g-C_3N_4/Ag/TiO_2 microspheres.

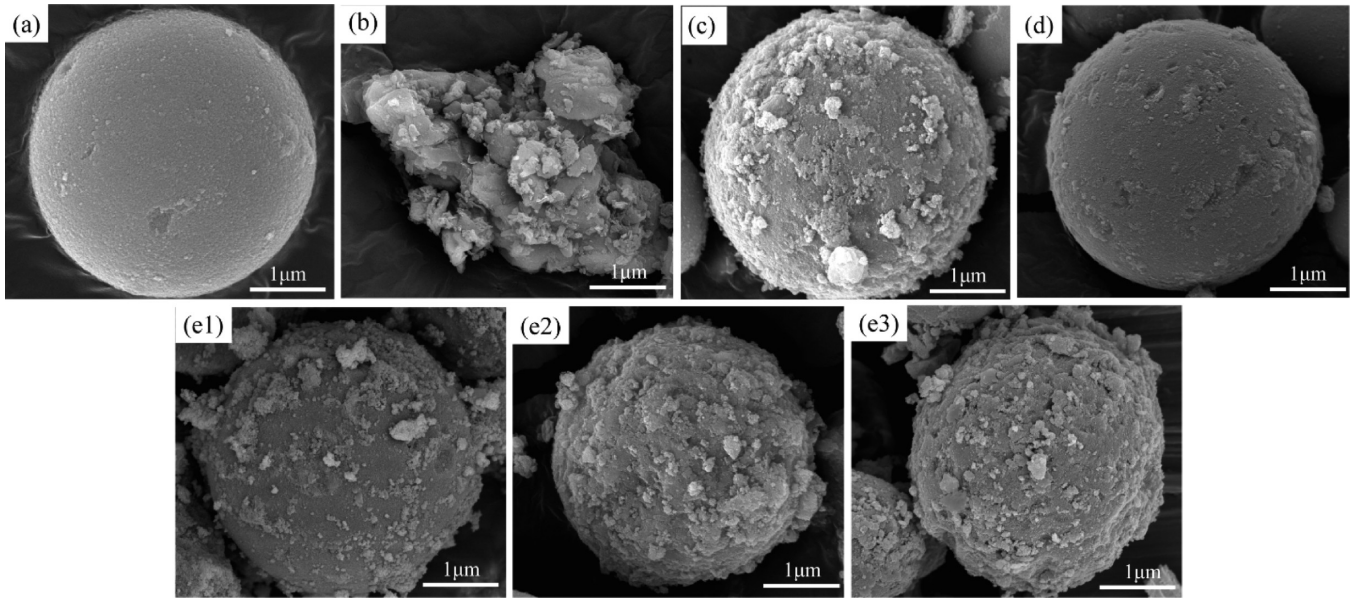

Figure 3. FE-SEM images of TiO_2 microspheres (a), protonated g-C_3N_4 (b), g-C_3N_4/TiO_2 microspheres (c), Ag/TiO_2 microspheres (d), g-C_3N_4 (2%)/Ag/TiO_2 microspheres (e1), g-C_3N_4 (4%)/Ag/TiO_2 microspheres (e2) and g-C_3N_4 (6%)/Ag/TiO_2 microspheres (e3).

For further investigating the heterostructured g-C_3N_4/Ag/TiO_2 microspheres, TEM characterization was performed. The g-C_3N_4 (4%)/Ag/TiO_2 microspheres were embedded in resin and ultrathin cross sections of the composite microspheres were observed by TEM. Figure 4A,B shows the broken g-C_3N_4/Ag/TiO_2 microsphere cross sections. A three-layer composite structure was clearly observed, which included g-C_3N_4 as the outer layer (in close to the embedding resin) with a thickness of about 80 nm, Ag as the interlayer and TiO_2 as the inlayer. The nano-Ag particles have a size of about 5 nm (Figure 4D).

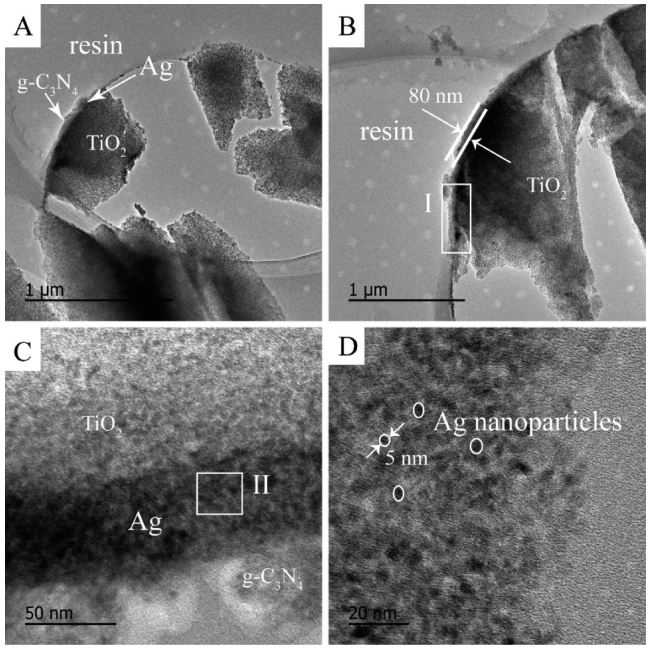

Figure 4. TEM images of the as-prepared g-C_3N_4 (4%)/Ag/TiO_2 microspheres photocatalyst: (A) and (B) broken ultrathin sections of g-C_3N_4 (4%)/Ag/TiO_2 microsphere, (C) enlarged view of area I and (D) enlarged view of area II.

FT-IR Analysis. The FT-IR spectrograms of the pure TiO_2 microspheres, protonated g-C_3N_4, g-C_3N_4/TiO_2 composite microspheres, Ag/TiO_2 composite microspheres and g-C_3N_4/Ag/TiO_2 composite microspheres are shown in Figure 5. For

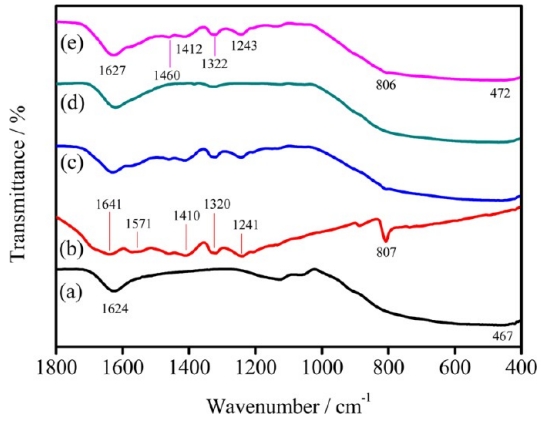

Figure 5. FT-IR spectra of TiO_2 microspheres (a), protonated g-C_3N_4 (b), g-C_3N_4/TiO_2 microspheres (c), Ag/TiO_2 microspheres (d) and g-C_3N_4 (4%)/Ag/TiO_2 microspheres (e).

pure TiO_2 microspheres, a wide absorption band appearing at 500−700 cm^{-1} is attributed to Ti−O stretching.[25] The peak appearing at 1624 cm^{-1} is attributed to the bending vibration of O−H.[29] The pure g-C_3N_4 shows similar results to that described in previous report. As shown in Figure 5b, the absorption band at 1641 cm^{-1} can be ascribed to the C−N heterocycle stretching vibration modes, whereas the four strong peaks at 1241, 1320, 1410 and 1571 cm^{-1} can be assigned to aromatic C−N stretching vibration modes.[30,31] The peak at 807 cm^{-1} is associated with the characteristic breathing mode of triazine units.[32,33] The Ag/TiO_2 composite microspheres show similar absorption bands to the pure TiO_2 microspheres. Furthermore, it can be evidently shown that all of the main characteristic peaks of g-C_3N_4 and TiO_2 appeared in g-C_3N_4/TiO_2 composite microspheres and g-C_3N_4/Ag/TiO_2 micro-

dx.doi.org/10.1021/am503674e | ACS Appl. Mater. Interfaces 2014, 6, 14405−14414

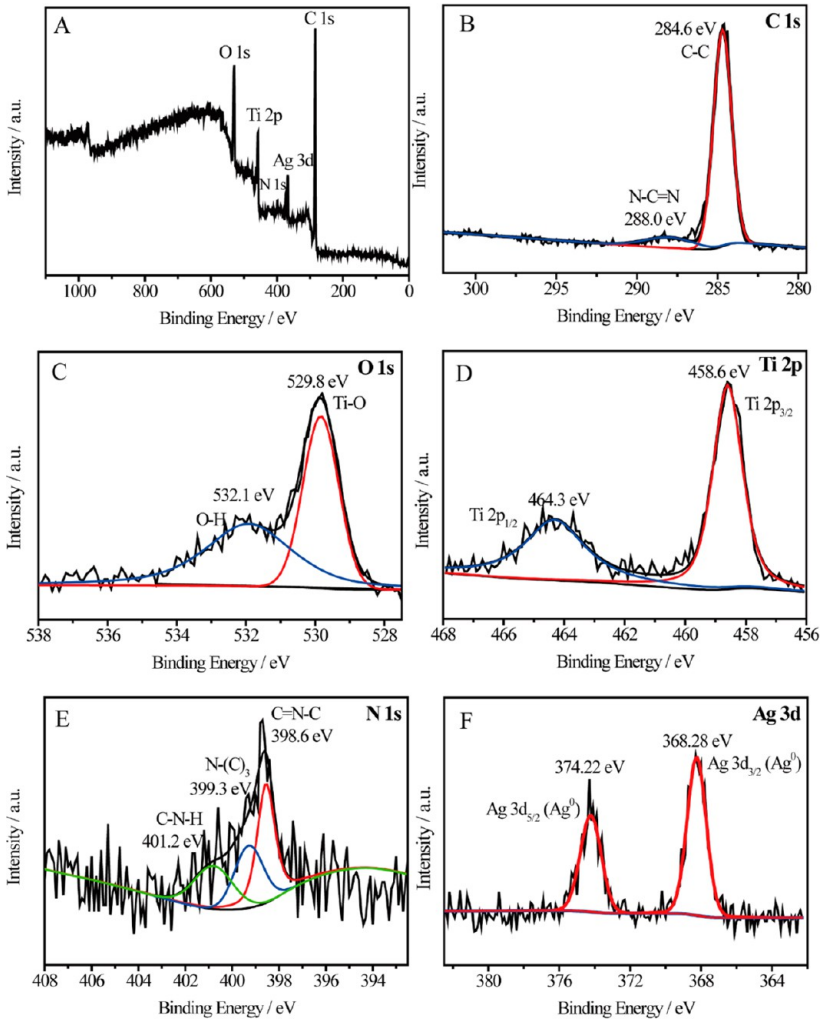

Figure 6. X-ray photoelectron spectra (XPS) survey spectrum of g-C_3N_4 (4%)/Ag/TiO_2 microspheres (A), high-resolution spectra of the C 1s (B), O 1s (C), Ti 2p (D), N 1s (E) and Ag 3d (F) for g-C_3N_4 (4%)/Ag/TiO_2 sample.

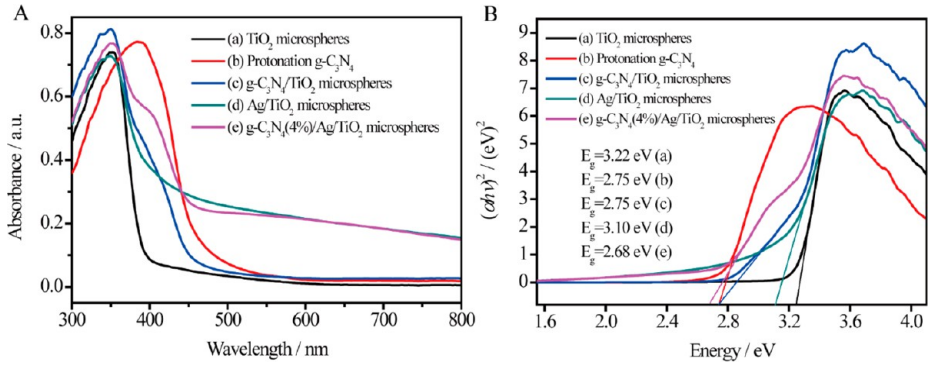

Figure 7. UV−vis absorption spectra (A) and the corresponding Kubelka−Munk transformed reflectance spectra (B) of TiO_2 microspheres (a), protonated g-C_3N_4 (b), g-C_3N_4/TiO_2 microspheres (c), Ag/TiO_2 microspheres (d) and g-C_3N_4 (4%)/Ag/TiO_2 microspheres (e).

spheres (Figure 5c,e). The condensation reaction between NH-groups on g-C_3N_4 and hydroxyl groups on TiO_2 microspheres was possible in the heating condition at 70°.[34]

XPS Spectra of g-C_3N_4/Ag/TiO_2 Microspheres. XPS analysis was carried out to further analyze the surface chemical composition and chemical status of elements in the as-prepared g-C_3N_4/Ag/TiO_2 microsphere sample (Figure 6). The peak positions in all of the XPS spectra were calibrated with C 1s at 284.6 eV. Figure 6A shows the XPS survey spectrum of the g-C_3N_4/Ag/TiO_2 microsphere sample, which indicates the sample primarily consists of C, Ag, N, Ti and O elements. The C 1s, Ag 3d, N 1s, Ti 2p and O 1s could be easily observed in the survey spectra. Figure 6B illustrates the high-resolution C 1s spectrum of the g-C_3N_4/Ag/TiO_2 microsphere sample. It can be seen that the sample has two C 1s peaks located at 284.6 and 288.0 eV. The former is strong and attributed to C—C coordination including the adventitious hydrocarbon from the XPS instrument itself and sp^2-hybridized carbon atoms present

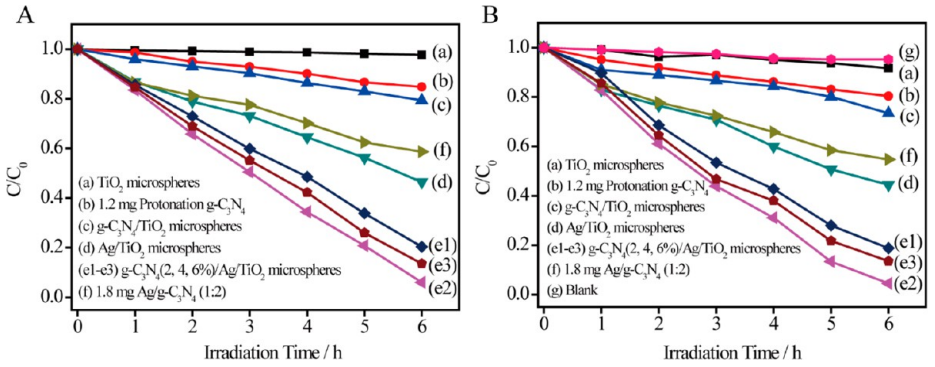

Figure 8. Photocatalytic activities of TiO_2 microspheres (a), protonated g-C_3N_4 (b), g-C_3N_4/TiO_2 microspheres (c), Ag/TiO_2 microspheres (d), g-C_3N_4 (2, 4 and 6%)/Ag/TiO_2 microspheres (e1−e3) and 1.8 mg Ag/g-C_3N_4 (1:2) (f) on the degradation of methyl orange (A) and phenol (B) under visible-light irradiation (λ>420 nm).

in g-C_3N_4, whereas the latter one is assigned to N—C═N coordination.[35] The O 1s high-resolution spectrum in Figure 6C can be fitted into two peaks, corresponding to the Ti—O bond (529.8 eV) and O—H bond (532.1 eV).[36] The O 1s peak at 532.1 eV is related to the presence of a hydroxyl group or water molecule on the surface of the g-C_3N_4/Ag/TiO_2 composite microspheres, which is corresponding with the FT-IR results in Figure 5. From Figure 6D, the Ti 2p spectrum shows two peaks at binding energy of 458.6 (Ti $2p_{3/2}$) and 464.3 eV (Ti $2p_{1/2}$), respectively. The N 1s high-resolution spectrum in Figure 6E can be fitted into three peaks, which belongs to C═N—C at 398.6 eV, N—$(C)_3$ at 399.3 eV and C—N—H at 401.2 eV, respectively.[37] As shown in Figure 6F, typical peaks of Ag 3d can be found, in which the peaks at 368.3 and 374.2 eV are ascribed to Ag $3d_{3/2}$ (Ag^0) and Ag $3d_{5/2}$ (Ag^0) and the result is in accordance with previous reports.[38,39]

UV−Vis Diffuses Reflectance Spectra. The absorbance properties of the as-prepared samples were measured using UV−vis diffuse reflectance spectroscopy. Figure 7A displays the UV−vis diffuse reflectance spectra of the g-C_3N_4/TiO_2 composite microspheres, Ag/TiO_2 composite microspheres and g-C_3N_4 (4%)/Ag/TiO_2 composite microspheres, together with those of pure TiO_2 microspheres and protonated g-C_3N_4. For the pure TiO_2 microspheres, the basal absorption edge occurs at wavelength shorter than 390 nm (Figure 7A (a), whereas the absorption intensity of protonated g-C_3N_4 rises rapidly at about 460 nm (Figure 7A (b)). After g-C_3N_4 is wrapped on TiO_2 microspheres, the optical absorption of g-C_3N_4/TiO_2 composite microspheres is enhanced, distinctly in the visible light zone (Figure 7A (c)). Compared to pure TiO_2 microspheres, the g-C_3N_4 (4%)/TiO_2 composite microspheres show obvious additional absorption in the 390−460 nm region and the absorption edge occurs at a wavelength of about 460 nm, which was because of the existence of g-C_3N_4 on the large surface area of TiO_2 microspheres. As shown in Figure 7A (d), Ag/TiO_2 composite microspheres show obvious visible-light absorption, which can be attributed to the surface plasmon resonance (SPR) of the loading Ag, further confirming the formation of Ag nanoparticles.[28] Meanwhile, the absorption edge of Ag/TiO_2 microspheres with a slight red shift have also been detected. The absorption curve of the ternary composite of heterostructured g-C_3N_4/Ag/TiO_2 microspheres shows distinctly enhanced visible-light absorption as compared to the pure TiO_2 microspheres, g-C_3N_4/TiO_2 composite microspheres and Ag/TiO_2 composite microspheres. The absorption edge of g-C_3N_4/Ag/TiO_2 composite microspheres has a remarkable red shift to a higher wavelength at about 480 nm. The band gap energies of semiconductors can be estimated by Kubelka−Munk transformation, $\alpha h\upsilon = A(h\upsilon - E_g)^{n/2}$, where α represents the absorption coefficient, υ is the light frequency, E_g is the band gap energy, A is a constant and n depends on the characteristics of the transition in a semiconductor.[40,41] For g-C_3N_4 and TiO_2, the value of n is 4 for the indirect transition. Thus, as shown in Figure 7B, the band gap energies (E_g) of pure TiO_2 microspheres, protonated g-C_3N_4, g-C_3N_4/TiO_2 composite microspheres, Ag/TiO_2 composite microspheres and g-C_3N_4/Ag/TiO_2 composite microspheres are calculated to be 3.22, 2.75, 2.75, 3.10, and 2.68 eV, respectively. The potentials of VB and CB of a semiconductor material can be estimated according to the following empirical equations:

$$E_{VB} = \chi - E^e + 0.5E_g$$

$$E_{CB} = E_{VB} - E_g$$

where E_{VB} is the valence band edge potential, χ is the electronegativity of the semiconductor, which is the geometric mean of the constituent atoms, E^e is the energy of free electrons on the hydrogen scale (about 4.5 eV vs NHE) and E_g is the band gap energy of the semiconductor. The χ-values for g-C_3N_4 and TiO_2 are 4.64 and 5.81 eV, respectively. The E_{VB} of g-C_3N_4 and TiO_2 are calculated to be 1.52 and 2.92 eV, respectively. The E_{CB} of g-C_3N_4 and TiO_2 are estimated to be −1.23 and −0.30 eV, respectively.

Photocatalytic Performance. Figure 8A displays the photocatalytic decolorization of MO over different photocatalysts. On the basis of a blank experiment, the self-photolysis of MO could be neglected. For a pure TiO_2 microsphere sample and 1.2 mg of protonated g-C_3N_4 (identical mass of g-C_3N_4 in 30 mg of g-C_3N_4 (4%)/Ag/TiO_2), the concentration of MO is only reduced by about 2.3 and 15.3% after 6 h of visible-light irradiation. Two-component composites containing g-C_3N_4/TiO_2, Ag/TiO_2 and 1.8 mg of Ag/g-C_3N_4 (sum mass of g-C_3N_4 and Ag in 30 mg of g-C_3N_4 (4%)/Ag/TiO_2) show higher photocatalytic activity, and the concentrations of MO are reduced by about 20.7, 53.5 and 41.4%, respectively. Compared with the single-component samples and two-component samples, the ternary composite of heterostructured g-C_3N_4 (2, 4 and 6%)/Ag/TiO_2 microsphere samples exhibit remarkably enhanced photocatalytic activity, which the concentration of MO is reduced by about 79.7, 94.0 and 86.4%, respectively. It should be noted that g-C_3N_4 (4%)/Ag/TiO_2 microsphere sample shows higher photocatalytic activity

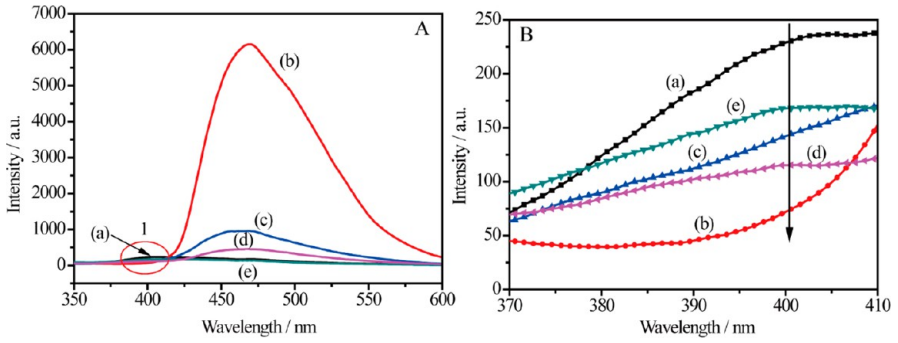

Figure 9. Photoluminescence (PL) spectra of TiO_2 microspheres (a), protonated g-C_3N_4 (b), g-C_3N_4/TiO_2 microspheres (c), Ag/TiO_2 microspheres (d), g-C_3N_4 (4%)/Ag/TiO_2 microspheres (e) (A) and the magnified spectra of area 1 (B).

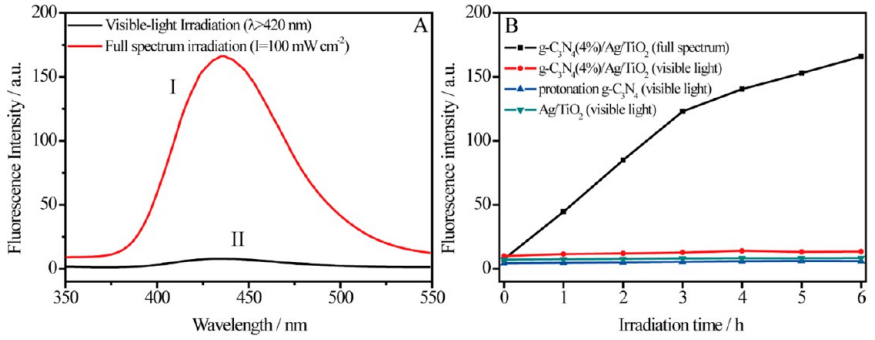

Figure 10. (A) PL spectral of g-C_3N_4/Ag/TiO_2 microsphere sample in 2 mM NaOH solution in the presence of 0.5 mM terephthalic acid observed under Xe lamp irradiation (full spectrum, I = 100 mW cm^{-2}) (I) and under visible-light irradiation (λ>420 nm) (II) at the illumination time of 6 h. (B) Comparison of PL intensity at 435 nm against irradiation time for protonated g-C_3N_4, Ag/TiO_2 microspheres and g-C_3N_4/Ag/TiO_2 microspheres under visible-light irradiation (λ>420 nm), together with g-C_3N_4/Ag/TiO_2 microspheres under Xe lamp irradiation (full spectrum, I = 100 mW cm^{-2}).

than the sum of 1.2 mg g-C_3N_4 and Ag/TiO_2 samples (68.8%), or the sum of TiO_2 and 1.8 mg Ag/g-C_3N_4 samples (43.7%). As interlayers, Ag nanoparticles inside the samples participate in electrical conduction and bridge the gap between g-C_3N_4 andTiO_2, facilitating the separation of photoexcited charge and reducing the recombination of the photogenerated electron−hole. During the photocatalysis characterization of the g-C_3N_4 (4%)/Ag/TiO_2 microsphere sample, the concentration of total organic carbon (TOC) for MO was evaluated, and the results are illustrated in Figure S4 (Supporting Information). Obviously, the rate of decolorization was much faster than that of mineralization. The TOC value of MO is reduced by about 30.9% after 6 h of visible-light irradiation, which shows the evidence of the decomposition of MO into carbon dioxide but at a relatively slow rate. Furthermore, considering the sensitization effect, a colorless organic compound, phenol, has been used for photodegradation studies (Figure 8B). The experimental results for phenol degradation under the same conditions clearly demonstrate that the photocatalytic activity is consistent with the trend for the MO degradation.

Nitrogen adsorption−desorption analysis was used to determine surface areas (Brunauer−Emmett−Teller (BET) method) of the catalysts (Table S1 and Figure S3, Supporting Information). As shown in Table S1 (Supporting Information), the surface area of Ag/TiO_2 microspheres was calculated to be 228.29 m^2 g^{-1}, which was similar to that of the nonsilver containing TiO_2. But g-C_3N_4 had an opposite effect on the surface area of the composite samples. Low content of g-C_3N_4 (2%) in g-C_3N_4/Ag/TiO_2 microspheres had a larger surface area but lower photocatalytic activity than the g-C_3N_4 (4%)/Ag/TiO_2 microsphere sample. The reason is that the low content of g-C_3N_4 can only generate a few electron−hole pairs, resulting in lower photocatalytic activity. When the content of g-C_3N_4 increased to 6%, the decreased surface area limited the contact chance between pollutant and photocatalyst, which reduced the rate of the photocatalytic reaction.

Photocatalytic Mechanism of the Heterostructured g-C_3N_4/Ag/TiO_2 Microspheres. The recombination of electron−hole pairs can release energy, which can be detected by PL emission. A lower PL intensity is a general indication of a lower recombination of electron−hole pairs, resulting in higher photocatalytic activity.[42] As g-C_3N_4 and TiO_2 have different emission peaks, and they were compared with g-C_3N_4/TiO_2 microspheres, Ag/TiO_2 microspheres and g-C_3N_4 (4%)/Ag/TiO_2 microspheres in different wavelength ranges, which are shown in Figure 9A,B. The PL spectra of protonated g-C_3N_4 have a strong emission peak at around 460 nm, which is assigned to the recombination of the photoinduced electron−holes of g-C_3N_4. In comparison with the protonated g-C_3N_4, the intensities of the peaks for g-C_3N_4/TiO_2 microspheres, Ag/TiO_2 microspheres and g-C_3N_4 (4%)/Ag/TiO_2 microspheres are much lower, which reveals that the composites have a lower recombination rate of electron−hole pairs. The g-C_3N_4 (4%)/Ag/TiO_2 microsphere sample, in particular, demonstrates almost no emission peak at the position of 460 nm, suggesting the lowest recombination rate of photoinduced electron−hole pairs. In the emission peak at about 400 nm, the photoluminescence intensities of g-C_3N_4/TiO_2 microspheres, Ag/TiO_2 microspheres and g-C_3N_4 (4%)/Ag/TiO_2 microspheres

are always lower than that of the pure TiO_2 microsphere sample, which means that the separation of photoinduced electrons and holes in the g-C_3N_4/TiO_2 microspheres, Ag/TiO_2 microspheres and g-C_3N_4 (4%)/Ag/TiO_2 microspheres were more efficient than that of the pure TiO_2 microsphere sample. The highest photoactivity of the g-C_3N_4 (4%)/Ag/TiO_2 microsphere sample was consistent with its highest charge-separation efficiency. The PL results evidence the importance of the heterostructure of g-C_3N_4–Ag–TiO_2 in blocking the recombination of electrons and holes.

To further investigate the photocatalytic mechanism of the g-C_3N_4/Ag/TiO_2 microspheres, the trapping experiment of hydroxyl radicals was carried out in the photocatalytic process. Hydroxyl radicals (·OH) were measured on the surface of g-C_3N_4/Ag/TiO_2 microspheres under full spectrum irradiation and protonated g-C_3N_4, Ag/TiO_2 microspheres and g-C_3N_4/Ag/TiO_2 microspheres were measured under visible-light (λ > 420 nm) irradiation by the PL method using terephthalic acid as a probe molecule. Figure 10 shows the PL spectral of g-C_3N_4/Ag/TiO_2 microsphere sample under different irradiation conditions at the illumination time of 6 h. Obviously, the PL signal is strong and the intensity enhances gradually with increasing irradiation time on the full spectrum irradiation, which indicates the production of ·OH radicals. The PL signal, however, is weak on the visible-light irradiation, implying that no hydroxyl radicals were produced in the photocatalytic process. In the cases of protonated g-C_3N_4, Ag/TiO_2 microspheres and g-C_3N_4/Ag/TiO_2 microsphere samples on visible-light irradiation (λ > 420 nm), there is no change in PL intensity at 435 nm under a long irradiation time. The data demonstrate the ·OH radicals were not the major oxygen species. In other words, under the visible-light photochemical process, the holes on the TiO_2 surface in the g-C_3N_4/Ag/TiO_2 sample could not be generated, because the holes in the VB of TiO_2 (2.92 eV) locate at lower potential positions than the OH^-/·OH couple (2.70 eV), which could oxidize OH^- or H_2O to form ·OH.

On the basis of the results and discussion above, the photocatalytic mechanism for the g-C_3N_4/Ag/TiO_2 microspheres is proposed and schematically exhibited in Figure 11. Given the calculation results above, the CB and VB edge potentials of g-C_3N_4 were at −1.23 and +1.52 eV, whereas the CB and VB edge potentials of TiO_2 were at −0.30 and +2.92 eV, respectively. Under visible-light irradiation, only g-C_3N_4 absorbed visible light and excited. Because the CB edge of g-C_3N_4 is more negative than that of TiO_2, the photoinduced electrons on g-C_3N_4 can transfer easily to the CB of TiO_2. In the system of g-C_3N_4/Ag/TiO_2 microspheres, nano-Ag particles were deposited on the surface of TiO_2 microspheres and played an important role as an electron-conduction bridge. The electrons transfer toward TiO_2 and electron–holes separation in g-C_3N_4 would be more efficient because of the formed Schottky barrier at the interface of Ag and TiO_2 nanoparticles.[34] The photoinduced electrons of g-C_3N_4 directionally migrate to Ag/TiO_2 due to the close interfacial connections between Ag/TiO_2 and g-C_3N_4 where photoinduced electrons and holes are efficiently separated in space, which is conducive to retarding the recombination of electron–holes and improving the photoactivity. On the other hand, the surface plasmon resonance of nano-Ag particles can enhance visible-light absorption. As the electrons in CB of TiO_2 (−0.30 eV) locate at more negative potential positions than the O_2/·O_2^- couple (−0.046 eV), electrons stored in the CB of TiO_2 are trapped by O_2 dissolved in the solution near the surface of TiO_2 to generate reactive superoxide radical ions (·O_2^-), while the holes in the VB of g-C_3N_4 directly oxidize the pollutants. Notably, the content of g-C_3N_4 in g-C_3N_4/Ag/TiO_2 microspheres should be controlled at an optimal value, because the main degradation process took place on the surface of TiO_2 and dissolved O_2 and the pollutant molecules had to travel through the outer layer composed by g-C_3N_4. Therefore, it is not surprising that the higher content (6%) of g-C_3N_4 leads to a lower photocatalytic activity than that of the content of 4% (Figure 8e1–e3).

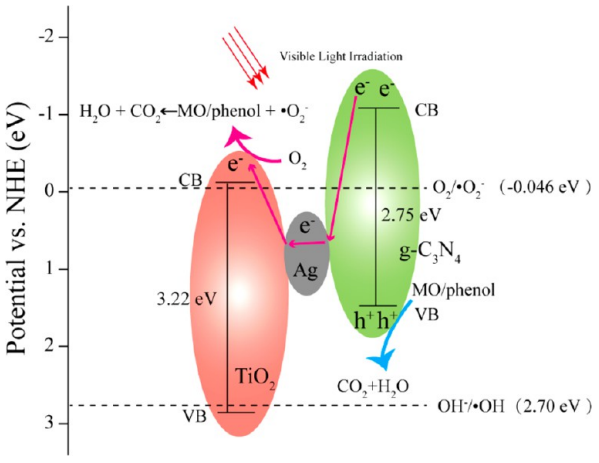

Figure 11. Photocatalytic Mechanism Scheme of g-C_3N_4/Ag/TiO_2 microspheres under visible light irradiation (>420 nm).

Recyclability of g-C_3N_4 (4%)/Ag/TiO_2 Microsphere Sample. For evaluating the recyclability of the g-C_3N_4 (4%)/Ag/TiO_2 microsphere sample, the additional experiments have been carried out to degrade MO under visible light cycled for four times (Figure 12). The photocatalytic activity of g-C_3N_4 (4%)/Ag/TiO_2 microsphere sample for MO degradation decreased from 94.0% to 86.5% after four cycling runs, which demonstrates that the g-C_3N_4 (4%)/Ag/TiO_2 microsphere sample has high stability in the photocatalytic process under visible-light irradiation. Furthermore, there is no obvious difference in SEM images (Figure S5, Supporting Information) and XRD patterns (Figure S6, Supporting Information) of photocatalysts after the first cycle measurement. XPS analysis was also performed to further analyze the surface chemical composition and chemical status of elements in the g-C_3N_4

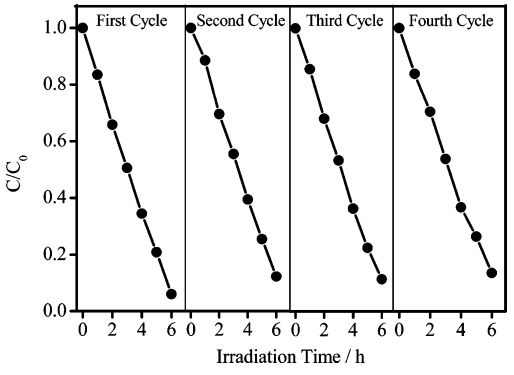

Figure 12. Cycle runs of g-C_3N_4/Ag/TiO_2 microspheres for degradation of MO under visible-light irradiation (λ > 420 nm).

(4%)/Ag/TiO_2 microsphere sample after the photocatalytic measurement (Figure S7, Supporting Information). Difference can be observed from high-resolution spectrum of C 1s, O 1s and N 1s. The C−O and NO_x groups can be ascribed to the residual photocatalytic product from the incomplete mineralization of MO.[43,44]

4. CONCLUSIONS

In summary, heterostructured g-C_3N_4/Ag/TiO_2 microsphere samples have been successfully constructed via an easily accessible route. During this process, Ag/TiO_2 microspheres were first synthesized by a photodeposition method, followed by encapsulating g-C_3N_4 on Ag/TiO_2 microspheres, and its structural and photocatalytic properties were studied. The resulting g-C_3N_4 (4%)/Ag/TiO_2 microsphere sample shows significantly enhanced photocatalytic activity (94.0%) toward degradation of methyl orange under visible-light irradiation, as compared with the sum of 1.2 mg g-C_3N_4 and Ag/TiO_2 samples (68.8%), or the sum of TiO_2 and 1.8 mg Ag/g-C_3N_4 samples (43.7%). Experimental results indicate that the close interfacial connections between Ag/TiO_2 and g-C_3N_4, where photoinduced electrons and holes were efficiently separated in space, were conductive to retarding the charge recombination and improving the photoactivity. The nano-Ag particles deposited on the surface of TiO_2 microspheres in the g-C_3N_4/Ag/TiO_2 composite play an important role as an electron-conduction bridge; the electrons transfer toward TiO_2 and electron−holes separation in g-C_3N_4 would be more efficient. The main degradation process took place on the surface of TiO_2 and dissolved O_2 and consequently, the pollutants had to travel through the outer layer composed by g-C_3N_4, which a higher content (6%) of g-C_3N_4 leads to a lower photocatalytic activity than that of the content of 4%. Moreover, the g-C_3N_4/Ag/TiO_2 microsphere sample exhibited good recyclability under visible-light irradiation. On the basis of the results of this study, the g-C_3N_4/Ag/TiO_2 microsphere sample is expected to be effective as a useful visible-light photocatalyst for practical applications.

ASSOCIATED CONTENT

Supporting Information

SEM images of TiO_2 microspheres surface and Ag/TiO_2 microspheres surface, survey SEM image of g-C_3N_4 (4%)/Ag/TiO_2 microspheres, nitrogen adsorption−desorption isotherms, BET surface areas of the as-prepared samples, photocatalytic activity of g-C_3N_4 (4%)/Ag/TiO_2 microspheres, SEM image of g-C_3N_4 (4%)/Ag/TiO_2 microspheres after the photocatalytic measurement, XRD pattern of g-C_3N_4 (4%)/Ag/TiO_2 microspheres after the photocatalytic measurement and XPS survey spectrum. This material is available free of charge via the Internet at http://pubs.acs.org.

AUTHOR INFORMATION

Corresponding Authors

*Y. Situ. Tel./fax: +86-020-87112093. E-mail: situyue@scut.edu.cn.

*H. Huang. Tel./fax: +86-020-87112093. E-mail: cehhuang@scut.edu.cn.

Notes

The authors declare no competing financial interest.

ACKNOWLEDGMENTS

The authors gratefully thank the "National Nature Science Foundation of China (No. 51103045)" for financial support of this work.

REFERENCES

(1) Sastre, F.; Puga, A. V.; Liu, L.; Corma, A.; Garcia, H. Complete Photocatalytic Reduction of CO_2 to Methane by H_2 under Solar Light Irradiation. *J. Am. Chem. Soc.* **2014**, *136*, 6798−6801.

(2) Lin, C. H.; Chao, J. H.; Liu, C. H.; Chang, J. C.; Wang, F. C. Effect of Calcination Temperature on the Structure of a Pt/TiO_2 (B) Nanofiber and Its Photocatalytic Activity in Generating H_2. *Langmuir* **2008**, *24*, 9907−9915.

(3) Zhang, Y. H.; Tang, Z. R.; Fu, X. Z.; Xu, Y. J. TiO_2-Graphene Nanocomposites for Gas-Phase Photocatalytic Degradation of Volatile Aromatic Pollutant: Is TiO_2-Graphene Truly Different from Other TiO_2-Carbon Composite Materials? *ACS Nano* **2010**, *4*, 7303−7314.

(4) Subramanian, V.; Wolf, E.; Kamat, P. V. Semiconductor-Metal Composite Nanostructures. To what Extent do Metal Nanoparticles Improve the Photocatalytic Activity of TiO_2 Films? *J. Phys. Chem. B* **2001**, *105*, 11439−11446.

(5) Wu, Y. C.; Ju, L. S. Annealing-free Synthesis of C-N Co-Doped TiO_2 Hierarchical Spheres by Using Amine Agents via Microwave-Assisted Solvothermal Method and Their Photocatalytic Activities. *J. Alloys Compd.* **2014**, *604*, 164−170.

(6) Li, S. X.; Zheng, F. Y.; Cai, S. J.; Liang, W. J.; Li, Y. C. A Visible Light Assisted Photocatalytic System for Determination of Chemical Oxygen Demand Using 5-Sulfosalicylic Acid in Situ Surface Modified Titanium Dioxide. *Sens. Actuators, B* **2013**, *188*, 280−285.

(7) Baker, D. R.; Kamat, P. V. Photosensitization of TiO_2 Nanostructures with CdS Quantum Dots: Particulate versus Tubular Support Architectures. *Adv. Funct. Mater.* **2009**, *19*, 805−811.

(8) Campbell, W. M.; Burrell, A. K.; Officer, D. L.; Jolley, K. W. Porphyrins as Light Harvesters in the Dye-Sensitised TiO_2 Solar Cell. *Coord. Chem. Rev.* **2004**, *248*, 1363−1379.

(9) Gu, L. A.; Wang, J. Y.; Zou, Z. J.; Han, X. J. Graphitic-C_3N_4-Hybridized TiO_2 Nanosheets with Reactive {001} Facets to Enhance the UV- and Visible-Light Photocatalytic Activity. *J. Hazard. Mater.* **2014**, *268*, 216−223.

(10) Sridharan, K.; Jang, E.; Park, T. J. Novel Visible Light Active Graphitic C_3N_4-TiO_2 Composite Photocatalyst: Synergistic Synthesis, Growth and Photocatalytic Treatment of Hazardous Pollutants. *Appl. Catal., B* **2013**, *142*, 718−728.

(11) Miranda, C.; Mansilla, H.; Yanez, J.; Obregon, S.; Colon, G. Improved Photocatalytic Activity of g-C_3N_4/TiO_2 Composites Prepared by a Simple Impregnation Method. *J. Photochem. Photobiol., A* **2013**, *253*, 16−21.

(12) Zhao, S. S.; Chen, S.; Yu, H. T.; Quan, X. g-C_3N_4/TiO_2 Hybrid Photocatalyst with Wide Absorption Wavelength Range and Effective Photogenerated Charge Separation. *Sep. Purif. Technol.* **2012**, *99*, 50−54.

(13) Wang, J. X.; Huang, J.; Xie, H. L.; Qu, A. L. Synthesis of g-C_3N_4/TiO_2 with Enhanced Photocatalytic Activity for H_2 Evolution by a Simple Method. *Int. J. Hydrogen Energy* **2014**, *39*, 6354−6363.

(14) Sakthivel, S.; Shankar, M. V.; Palanichamy, M.; Arabindoo, B.; Bahnemann, D. W.; Murugesan, V. Enhancement of Photocatalytic Activity by Metal Deposition: Characterisation and Photonic Efficiency of Pt, Au and Pd Deposited on TiO_2 Catalyst. *Water Res.* **2004**, *38*, 3001−3008.

(15) Zheng, Z. K.; Huang, B. B.; Qin, X. Y.; Zhang, X. Y.; Dai, Y.; Whangbo, M. H. Facile in Situ Synthesis of Visible-Light Plasmonic Photocatalysts M@TiO_2 (M = Au, Pt, Ag) and Evaluation of their Photocatalytic Oxidation of Benzene to Phenol. *J. Mater. Chem.* **2011**, *21*, 9079−9087.

(16) Liang, W. J.; Li, J.; Jin, Y. Q. Photo-Catalytic Degradation of Gaseous Formaldehyde by TiO_2/UV, Ag/TiO_2/UV and Ce/TiO_2/UV. *Build. Environ.* **2012**, *51*, 345−350.

(17) Atrei, A.; Ferrari, A. M.; Szieberth, D.; Cortigiani, B.; Rovida, G. Lepidocrocite-like Structure of the TiO_2 Monolayer Grown on Ag(100). *Phys. Chem. Chem. Phys.* **2010**, *12*, 11587−11595.
(18) Yan, S. C.; Li, Z. S.; Zou, Z. G. Photodegradation Performance of g-C_3N_4 Fabricated by Directly Heating Melamine. *Langmuir* **2009**, *25*, 10397−10401.
(19) Zhang, Y. J.; Thomas, A.; Antonietti, M.; Wang, X. C. Activation of Carbon Nitride Solids by Protonation: Morphology Changes, Enhanced Ionic Conductivity, and Photoconduction Experiments. *J. Am. Chem. Soc.* **2009**, *131*, 50−51.
(20) Zheng, Z. K.; Huang, B. B.; Qin, X. Y.; Zhang, X. Y.; Dai, Y. Strategic Synthesis of Hierarchical TiO_2 Microspheres with Enhanced Photocatalytic Activity. *Chem.—Eur. J.* **2010**, *16*, 11266−11270.
(21) Cheng, G.; Akhtar, M. S.; Yang, O. B.; Stadler, F. J. Novel Preparation of Anatase TiO_2@ Reduced Graphene Oxide Hybrids for High-performance Dye-sensitized Solar Cells. *ACS Appl. Mater. Interfaces* **2013**, *5*, 6635−6642.
(22) Xiang, Q.; Yu, J.; Jaroniec, M. Preparation and Enhanced Visible-Light Photocatalytic H_2-Production Activity of Graphene/C_3N_4 Composites. *J. Phys. Chem. C* **2011**, *115*, 7355−7363.
(23) Iliev, V.; Tomova, D.; Bilyarska, L.; Eliyas, A.; Petrov, L. Photocatalytic Properties of TiO_2 Modified with Platinum and Silver Nanoparticles in the Degradation of Oxalic Acid in Aqueous Solution. *Appl. Catal., B* **2006**, *63*, 266−271.
(24) Hosseini, M. G.; Shokri, M.; Khosravi, M.; Najjar, R.; Darbandi, M. Photodegradation of an Azo Dye by Silver-Doped Nano-Particulate Titanium Dioxide. *Toxicol. Environ. Chem.* **2011**, *93*, 1591−1601.
(25) Yu, J. G.; Wang, S. H.; Low, J. X.; Xiao, W. Enhanced Photocatalytic Performance of Direct Z-Scheme g-C_3N_4-TiO_2 Photocatalysts for the Decomposition of Formaldehyde in Air. *Phys. Chem. Chem. Phys.* **2013**, *15*, 16883−16890.
(26) An, T. C.; Chen, J. Y.; Nie, X.; Li, G. Y.; Zhang, H. M.; Liu, X. L.; Zhao, H. J. Synthesis of Carbon Nanotube-Anatase TiO_2 Submicrometer-sized Sphere Composite Photocatalyst for Synergistic Degradation of Gaseous Styrene. *ACS Appl. Mater. Interfaces* **2012**, *4*, 5988−5996.
(27) Groenewolt, M.; Antonietti, M. Synthesis of g-C_3N_4 Nanoparticles in Mesoporous Silica Host Matrices. *Adv. Mater.* **2005**, *17*, 1789−1792.
(28) Pan, X. Y.; Xu, Y. J. Defect-Mediated Growth of Noble-Metal (Ag, Pt, and Pd) Nanoparticles on TiO_2 with Oxygen Vacancies for Photocatalytic Redox Reactions under Visible Light. *J. Phys. Chem. C* **2013**, *117*, 17996−18005.
(29) Huang, T.; Huang, W. X.; Zhou, C.; Situ, Y.; Huang, H. Superhydrophilicity of TiO_2/SiO_2 Thin Films: Synergistic Effect of SiO_2 and Phase-Separation-induced Porous Structure. *Surf. Coat. Technol.* **2012**, *213*, 126−132.
(30) Zhang, J. S.; Zhang, M. W.; Zhang, G. G.; Wang, X. C. Synthesis of Carbon Nitride Semiconductors in Sulfur Flux for Water Photoredox Catalysis. *ACS Catal.* **2012**, *2*, 940−948.
(31) Kumar, S.; Surendar, T.; Baruah, A.; Shanker, V. Synthesis of a Novel and Stable g-C_3N_4-Ag_3PO_4 Hybrid Nanocomposite Photocatalyst and Study of the Photocatalytic Activity under Visible Light Irradiation. *J. Mater. Chem. A* **2013**, *1*, 5333−5340.
(32) Min, S. X.; Lu, G. X. Enhanced Electron Transfer from the Excited Eosin Y to mpg-C_3N_4 for Highly Efficient Hydrogen Evolution under 550 nm Irradiation. *J. Phys. Chem. C* **2012**, *116*, 19644−19652.
(33) Lotsch, B. V.; Schnick, W. From Triazines to Heptazines: Novel Nonmetal Tricyanomelaminates as Precursors for Graphitic Carbon Nitride Materials. *Chem. Mater.* **2006**, *18*, 1891−1900.
(34) Chai, B.; Peng, T. Y.; Mao, J.; Li, K.; Zan, L. Graphitic Carbon Nitride (g-C_3N_4)-Pt-TiO_2 Nanocomposite as an Efficient Photocatalyst for Hydrogen Production under Visible Light Irradiation. *Phys. Chem. Chem. Phys.* **2012**, *14*, 16745−16752.
(35) Singh, J. A.; Overbury, S. H.; Dudney, N. J.; Li, M. J.; Veith, G. M. Gold Nanoparticles Supported on Carbon Nitride: Influence of Surface Hydroxyls on Low Temperature Carbon Monoxide Oxidation. *ACS Catal.* **2012**, *2*, 1138−1146.
(36) Da Silva, L. A.; Alves, V. A.; De Castro, S. C.; Boodts, J. F. C. XPS Study of the State of Iridium, Platinum, Titanium and Oxygen in Thermally Formed IrO_2+TiO_2+PtO_x Films. *Colloids Surf., A* **2000**, *170*, 119−126.
(37) Seung Jae, Y.; Jung Hyun, C.; Gyu Hwan, O.; Kee Suk, N.; Chong Rae, P. Easy Synthesis of Highly Nitrogen-enriched Graphitic Carbon with a High Hydrogen Storage Capacity at Room Temperature. *Carbon* **2009**, *47*, 1585−1591.
(38) Ye, L. Q.; Liu, J. Y.; Gong, C. Q.; Tian, L. H.; Peng, T. Y.; Zan, L. Two Different Roles of Metallic Ag on Ag/AgX/BiOX (X = Cl, Br) Visible Light Photocatalysts: Surface Plasmon Resonance and Z-Scheme Bridge. *ACS Catal.* **2012**, *2*, 1677−1683.
(39) Chen, Z. H.; Wang, W. L.; Zhang, Z. G.; Fang, X. M. High-Efficiency Visible-Light-Driven Ag_3PO_4/AgI Photocatalysts: Z-Scheme Photocatalytic Mechanism for Their Enhanced Photocatalytic Activity. *J. Phys. Chem. C* **2013**, *117*, 19346−19352.
(40) In, S. I.; Vaughn, D. D.; Schaak, R. E. Hybrid CuO-$TiO_{2-x}N_x$ Hollow Nanocubes for Photocatalytic Conversion of CO_2 into Methane under Solar Irradiation. *Angew. Chem., Int. Ed.* **2012**, *51*, 3915−3918.
(41) Tauc, J. Absorption Edge and Internal Electric Fields in Amorphous Semiconductors. *Mater. Res. Bull.* **1970**, *5*, 721−730.
(42) Zhou, X.; Jin, B.; Li, L.; Peng, F.; Wang, H.; Yu, H.; Fang, Y. A Carbon Nitride/TiO_2 Nanotube Array Heterojunction Visible-Light Photocatalyst: Synthesis, Characterization, and Photoelectrochemical Properties. *J. Mater. Chem.* **2012**, *22*, 17900−17905.
(43) Pu, X.; Zhang, D.; Gao, Y.; Shao, X.; Ding, G.; Li, S.; Zhao, S. One-Pot Microwave-Assisted Combustion Synthesis of Graphene Oxide−TiO_2 Hybrids for Photodegradation of Methyl Orange. *J. Alloys Compd.* **2013**, *551*, 382−388.
(44) Li, H.; Guo, J.; Yang, L.; Lan, Y. Degradation of Methyl Orange by Sodium Persulfate Activated with Zero-Valent Zinc. *Sep. Purif. Technol.* **2014**, *132*, 168−173.